JOURNAL OF CATALYSIS 136, 342–360 (1992)

Kinetics of the CO/NO Surface Reactions by the Direct Observation of the Adsorbed Species

ERIC W. SCHARPF[1] AND JAY B. BENZIGER

Department of Chemical Engineering, Princeton University, Princeton, New Jersey 08544-5263

Received October 28, 1991; revised February 24, 1992

Dynamic reflection infrared spectroscopy (DRIRS) was used to characterize the adsorbed state dynamics of CO and NO during adsorption/desorption and the CO/NO reaction on a platinum foil. The adsorbed states of CO and NO were characterized by stretching vibrations in the 1400–2100 cm^{-1} range. A square wave modulated reactant source provided a flux of one species to the surface at a pressure equivalent of 10^{-7} to 10^{-5} mBar, while the background pressure of the other species was independently controlled. Sample temperatures were varied from 325 to 500 K. For CO adsorption, a single IR band was observed that shifted from 2040 to 2075 cm^{-1} with increasing coverage. In the CO adsorption/desorption experiments, two distinct kinetic regimes were observed. At temperatures below 420 K, where the CO coverages were high (>50% saturation) desorption was characterized by a rate constant $k = 10^5 e^{-7100/T_S} s^{-1}$. When the CO coverage was low, corresponding to the temperatures >450 K, the desorption rate constant was $k = 10^{15} e^{-18,000/T_S} s^{-1}$. The change in the effective rate constant for CO desorption is suggested to result from repulsive interactions between adsorbed CO molecules. Two NO absorption bands were observed at 1630 and 1770 cm^{-1} which were attributed to NO absorbed on restructured and relaxed Pt surfaces. The combination of surface restructuring and NO decomposition precluded the accurate determination of NO desorption kinetics. The presence of NO on the surface increased the rate at which CO was removed from the surface. The CO and NO reaction on the surface produced a maximum in the CO turnover rate dependent on the reactant pressure ratio, coverage, and temperature. Modulating the CO pressure affected the coverage of NO in both types of adsorption sites, and modulation of the NO pressure produced modulations in the CO coverage. Assuming a uniform surface reaction, the data for the rate constant of CO removal during the CO/NO reaction due to a CO pressure modulation with constant NO pressure or an NO pressure modulation with constant CO pressure were consistent with the rate-limiting step in the CO/NO reaction being a bimolecular surface reaction between adsorbed CO and adsorbed NO. The data were not consistent with NO dissociation being the rate-limiting reaction step. Alternative possibilities resulting from reactions at surface defects or more complex reaction mechanisms could also account for the data.

INTRODUCTION

The purpose of this work was to examine the processes of adsorption, surface reaction, and desorption as they occur in the reaction between adsorbed CO and NO on a platinum foil by monitoring the reactant concentrations on the surface with infrared spectroscopy. Platinum is used to catalyze the reaction

$$CO + NO \Rightarrow CO_2 + \tfrac{1}{2}N_2,$$

which is an important reaction in automobile catalytic converters. Both NO and CO possess well characterized infrared absorption bands that do not overlap so the adsorption, desorption, and reaction kinetics of CO and NO on platinum are observable with infrared spectroscopy.

Reflection infrared spectroscopy (RIRS) monitors the infrared absorption of molecular vibrations normal to the surface on highly reflecting substrates (*1*). The spectrometer used in this work is a continuous

[1] Present address: Air Products Corporation, Allentown, PA.

0021-9517/92 $5.00

wave apparatus with a prism monochromator (*2*). Electron energy loss spectroscopy (EELS) has also provided valuable information about the behavior of surface adsorbates (*3, 4*). Optical spectroscopy, as reported here, is not limited to UHV conditions which are necessary for EELS. Fourier transform infrared spectroscopy has also been extensively used to study adsorbates on metal surfaces, however, for certain dynamic characterizations, there is an advantage to the dispersive technique used in the studies reported here. For single wavelength experiments, continuous wave surface IR spectroscopy can collect data on a time scale as low as 10–40 msec, though an entire spectrum may take a minute to acquire. Fourier transform spectroscopy has the advantage of collecting complete spectra more rapidly than dispersive techniques; commercially available spectrometers can collect a spectrum with comparable signal to noise in ~1 sec. Recently Chabal and co-workers have employed a unique gating technique with a specially built interferometer to achieve ~10 msec time resolution with FTIR for single pulse adsorption experiments (*5*). This is exceptional work, but the approach is not easily adapted to examine perturbations to steady state kinetics. A second advantage of the polarization modulation technique employed here is the optical nulling of the ambient gas phase which allows clear and simple separation of the gas phase and adsorbed species.

The adsorption of CO on Pt has been the subject of many studies examining the energetics of adsorption/desorption (*6–12*), adsorption sites (*13–17*), and molecular vibrations (*18–21*). In summary, these studies have found that CO adsorbs associatively on Pt surfaces with a sticking probability of near unity (>0.5). The binding energy varies from circa 27 kcal/mol on the close-packed (111) (*8, 9, 10, 12*) surface to 36 kcal/mol on surfaces with lower Pt atoms coordination, such as Pt(100), Pt(110), or at defects such as steps (*6—10, 12*). On Pt(111) surfaces ordered structures are formed with CO occupying both 2-fold bridged sites and linear on-top sites. Defects, such as steps, inhibit long-range ordering precluding adsorption in bridged sites; on surfaces without extended (111) domains little or no bridged-bonded CO is observed (*10, 12, 14, 15*). Recently, Schweizer *et al.* (*16*) were able to calculate a potential energy curve linking the bridge and on top sites for CO on Pt(111) from the relative EELS absorption intensities of the two species in the 50–300 K temperature range. In another EELS experiment on Pt(111) at low temperature the energy differences between the CO bridge and on-top sites were determined as a function of coverage (*4*). Some dynamic diffusion experiments (FT-RIRS) on stepped (111) surfaces at low temperatures and low surface coverages have recently reported a diffusion activation energy of 4.4 kcal/mol with a pre-exponential factor of 8×10^9 sec^{-1} (*5*).

Extensive adsorption/desorption studies of NO on Pt surfaces have also been carried out (*22–25*). This research includes static reflection IR work with NO alone on platinum foils (*26–28*), EELS and IR studies on single crystals (*28–38*), and even some transmission IR with supported platinum catalysts (*39–41*). These studies have indicated the existence of three different NO species: bridge-bonded on (111) planes, on-top bonded on (111) planes, and on-top bonded to a restructured platinum surface. The lack of extended (111) domains has been found to inhibit bridge bonding of NO, similar to the effect seen with CO. In contrast to CO, NO has been observed to dissociate on Pt surfaces in UHV when defects such as steps are present (*38*).

CO and NO reactions on platinum surfaces have received significant attention over the past few years due to the large-scale use of catalytic converters for automotive exhaust control. Vibrational spectroscopy focused on CO/NO interactions on platinum single crystals (*24, 35, 37*) and supported catalysts (*39–42*) under static conditions. Some of the single crystal work has also indicated the presence of surface islanding

(*36*). Other TPD work has shown the Langmuir–Hinshelwood nature of the reaction on platinum (111) (*43*) and the existence of unusually rapid reaction characterized as "surface explosions" on polycrystalline platinum (*44*), Pt(100) (*36*), and Pt(410) (*37*). Furthermore, on the (100) surface, reaction rate oscillations have been observed (*45–47*).

The mechanism for the reaction between CO and NO is generally agreed to proceed by a Langmuir–Hinshelwood mechanism. Schmidt and co-workers studied the CO_2 product kinetics of the CO/NO reaction over a very broad range of pressures and temperatures and suggested that the reaction could always be described by a Langmuir–Hinshelwood reaction where the rate-limiting step was a bimolecular reaction between adsorbed CO and adsorbed NO (*50*). Most other studies have suggested that the rate-limiting step was the dissociation of NO under most conditions (*42, 43, 48, 49*). When excess NO was present the bimolecular reaction between CO and NO was proposed to be rate limiting (*44, 50, 51*). On Pt(100) the reaction is known to be further complicated by the surface structural transformation between the (5 × 20) "hexagonal" structure and the (1 × 1) square structure. This has been suggested to cause the surface explosions (*36, 46, 49*).

The reaction mechanism for the CO/NO reaction is not well characterized under dynamic reaction conditions. Thus far, the vast majority of experimental results have been dominated by low pressure and low temperature static studies exceedingly far removed from practical reaction conditions. The work presented in this paper, under dynamic conditions and moderate to high surface concentrations, considers conditions significantly closer to reaction conditions in a catalytic converter.

EXPERIMENTAL

The experiments consisted of directing a modulated gas beam at the sample surface with or without other reactant gases in the background. During the pressure modulation, the infrared absorption intensities of the different adsorbates were recorded as a function of time at various wavelengths. Experiments were conducted with different gas pressures and pressure ratios over a range of surface temperatures.

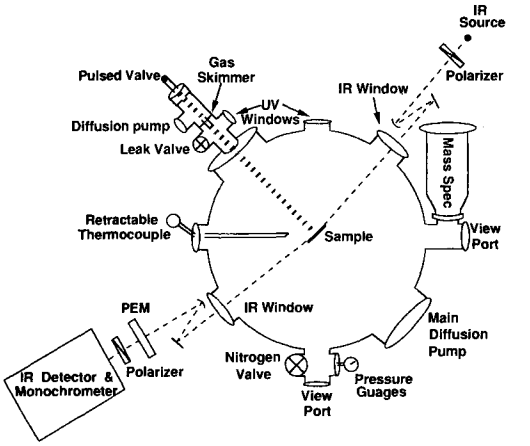

FIG. 1. Schematic of the scattering chamber.

The reflection infrared system measures the infrared absorption intensity of adsorbed species by monitoring the reflectivity difference between radiation polarized normal (p) and parallel (s) to the sample surface. The specifics of the design and construction of the spectrometer used in this study is detailed elsewhere (*2*). The configuration of the spectrometer with the modulated molecular beam system is shown in Fig. 1. The polarization modulation technique employed in these experiments acts as a double-beam spectrometer optically nulling the ambient gas phase. The spectrometer employed an HgCdTe/InSb sandwich detector. The HgCdTe detector covered the region 1360–1820 cm^{-1} with a noise level of 0.05% with a ≈50–100 msec response time, while the InSb part of the detector covered the 1860–4000 cm^{-1} range with <0.02% noise at response times of 10–20 msec. Dynamic experiments were sensitive to coverage changes as low as 0.001 monolayer of CO with a time resolution approaching 10 msec. A disadvantage with the HgCdTe/

InSb sandwich IR detector was that the bridge-bonded CO species at 1850 cm^{-1} was not detectable because its absorption peak fell in the center of the dark range of the detector. This was not a problem in the present study as bridge-bonded CO and NO have been found to be eliminated by the presence of steps and other defects which are present on the foil surface used in this work (*14, 15*). A few experiments were carried out with a broad band HgCdTe detector covering the range 1400–3000 cm^{-1} and we were never able to detect an absorption feature between 1800–1880 cm^{-1}. The sandwich detector was used for most studies because of the much greater sensitivity achieved with the InSb detector.

Samples were polished platinum foils, 15-mm square × 0.25-mm thick, cleaned by argon sputtering and annealed at 1000 K in an ion-pumped vacuum system ($P_{base} < 1 \times 10^{-9}$ mBar). Their cleanliness was verified with X-ray photoelectron spectroscopy prior to transfer to the reaction chamber. Before each different temperature run, the foil was sputtered and annealed to provide a fresh surface. This preparation procedure produced platinum surfaces with low levels of impurities (<10 atom%), and a nonnegligible defect concentration. The impurities were primarily due to adsorption of CO and residual hydrocarbons adsorbed during the time required to obtain an X-ray photoelectron spectrum. A more accurate measure of surface cleanliness was room temperature CO adsorption as discussed below.

For the molecular beam experiments the sample was transferred to the cryo-cooled diffusion pumped reaction chamber ($P_{base} = 1 \times 10^{-8}$ mBar), shown in Fig. 1. The reactants were delivered to the surface through a molecular beam source which consisted of a 100-cm^3 gas ballast vessel (not shown) connected to a pulsed valve from General Valve Corp. The valve has a 1-mm orifice and under computer control had a 2-msec response time to go fully open. A 100-mm long differentially pumped stage, pumped by a 175 l/sec cryotrapped diffusion pump, led to a 2-mm ID skimmer positioned 350 mm from the sample surface. Operating the valve with a 50% duty cycle at 0.25 Hz with a backing pressure in the ballast of 1.0–4.0 mBar yielded a 10^{-7}–10^{-6} mBar amplitude square wave pressure profile at the sample surface with a characteristic rise and fall time constant of roughly 50 msec as measured by a mass spectrometer placed in the sample position. Above 1 Hz the beam flux had to be reduced and was not sufficiently above the background pressure. At the sample, the beam diameter was approximately 30 mm, as measured by a mass spectrometer, assuring nearly uniform exposure of the Pt sample to the modulated beam. Beam fluxes were determined from the mass spectrometer signal when the ionizer was in the position of the Pt sample. The mass spectrometer signal at *m/e* 28 (CO) and *m/e* 30 (NO) were calibrated against known background pressures of CO and NO to determine the pressure equivalent of the molecular beam flux. A constant background gas was delivered through a variable leak valve. The CO and NO background flow pressures used in the NO/CO reaction experiments were varied from 1.3×10^{-7} mBar to 1.3×10^{-6} mBar.

Before beginning the dynamic experiments the sample at 300 K was exposed to CO at 10^{-6} mBar to saturate the surface with CO. An infrared spectrum was taken to determine the CO saturation coverage. This was used in addition to XPS as a measure of surface cleanliness. It also provided a normalization factor for the surface coverages for kinetic determinations. Small amounts of surface carbon contamination could reduce the CO saturation coverage by up to 20%. CO saturation coverage at room temperature was used as a measure of surface cleanliness. When the surface coverage fell by more than 20% it was deemed necessary to end the experiments and reclean the surface. By normalizing the coverages to the saturation coverage at 300 K these variations in fractional surface coverages were corrected for surface contamination. A

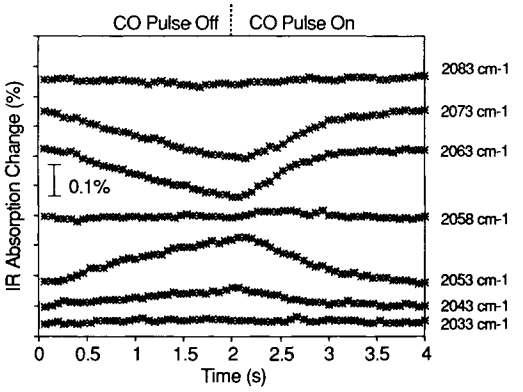

FIG. 2. Dynamic infrared spectra of CO adsorption/desorption on Pt foil at 0.25 Hz, 450 K, $\bar{p}_{CO} = 9.3 \times 10^{-7}$ mBar, $p_{CO}(\omega) = 7.2 \times 10^{-7}$ mBar.

second IR spectrum was taken after the dynamic experiment to determine the amount of contamination accumulated during the experiments. If the saturation coverage of CO changed by more than 5% after the dynamic experiments the data was not used for kinetic parameter determination.

Data in the DRIRS mode was taken by setting the spectrometer to the infrared frequency of interest then sampling the IR absorption intensity $I_s - I_p$ at 15 Hz. Monochromator entrance slit widths of 0.3 mm for the InSb detector and 0.8 mm for the HgCdTe detector were used which yielded resolutions of ~8 cm^{-1} at 2100 cm^{-1} and ~12 cm^{-1} at 1600 cm^{-1}. The monochromator was calibrated against a polystyrene standard and atmospheric CO_2. Sixteen waveforms were co-added to improve the signal to noise. The sample temperatures ranged from 325–490 K as measured by a thermocouple pushed in contact with the sample.

Full static reflection infrared spectra were taken of the adsorbates during the modulated experiments to obtain the average surface concentration of adsorbed species over a cycle. Spectral scan rates of ~2 cm^{-1}/sec were used. Two spectra phase shifted by 180° relative to the modulated gas beam were co-added to average out the cyclically changing surface coverage.

RESULTS

(i) CO Adsorption/Desorption

A typical set of dynamic spectra of CO adsorption/desorption at 450 K modulated at 0.25 Hz with a CO beam flux corresponding to 1.65×10^{-6} mBar is shown in Fig. 2, while the corresponding averaged spectrum is shown in Fig. 3. An important feature evident in Fig. 2 is the change in absorption as a function of wavelength was not monotonic with coverage. At infrared frequencies above 2058 cm^{-1} the absorption intensity increased as the CO coverage was increasing, as expected. In contrast the infrared absorption decreased with CO coverage at infrared frequencies below 2058 cm^{-1}. This behavior, where the infrared absorption intensity changed out-of-phase with the adsorbate concentration, results from the frequency of the infrared absorption band shifting as a function of adsorbate coverage. The CO absorption band shifts to higher frequency with increasing coverage due to dipole–dipole coupling of the CO molecules adsorbed on the surface and repulsive interactions between adsorbed molecules. The attenuating effects of the IR peak frequency shifting upward can overwhelm the increase in total peak amplitude resulting in the out-of-phase response of infrared intensity. In

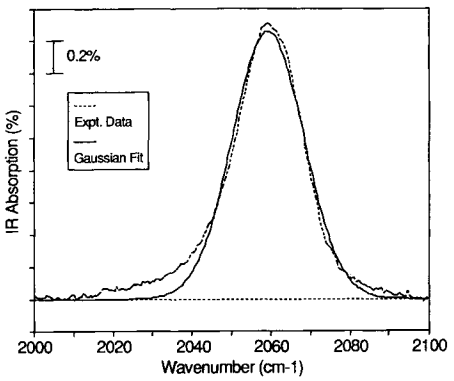

FIG. 3. Static infrared spectra of CO adsorption/desorption on Pt foil at 0.25 Hz, 453 K, $\bar{p}_{CO} = 9.3 \times 10^{-7}$ mBar, $p_{CO}(\omega) = 7.2 \times 10^{-7}$ mBar. Gaussian fit to the data is shown by solid line.

addition to causing the absorption to shift with coverage, the dipole–dipole coupling also reduces the absorption coefficient per molecule.

In order to extract the kinetics of adsorption/desorption and/or surface reaction the infrared absorption intensity data must be translated into surface coverages. The IR absorption peaks were very nearly gaussian in shape, as indicated in Fig. 3. The intensity, I, as a function of infrared frequency, ν, and surface coverage, θ, was approximated by a gaussian distribution,

$$I(\nu, \theta) = \frac{A(\theta)}{\sqrt{2\pi}\sigma} \exp\left\{ - \frac{(\nu - \bar{\nu}(\theta))^2}{2\sigma^2} \right\}, \quad (1)$$

where $A(\theta)$ is total integrated absorbance at coverage θ, $\bar{\nu}(\theta)$ is the frequency of the absorption maximum, and 2.4σ is the peak width at half maximum. The absorbance per molecule for CO on on-top adsorption sites is found from the integrated IR absorption intensity as a function of coverage. Bradshaw and Hayden have taken very complete LEED, thermal desorption, and infrared data for the adsorption of CO on Pt(111) (*13*). Below $\frac{1}{3}$ monolayer coverage, where the adsorbed CO molecules all occupy on-top sites, their data may be fit by a power law to give the number of adsorbed CO molecules in on-top adsorption sites, n_{CO}, where $I(\nu)\, d\nu$ has units %-cm^{-1}:

$$n_{CO} = 8.3 \times 10^{11} \{\int I(\nu)\, d\nu\}^{1.6} \text{ molecules/cm}^2. \quad (2)$$

We have obtained limited data correlating CO coverage as determined by X-ray photoelectron spectroscopy with integrated IR absorption on the Pt foil used in the experiments described here. The coverage determination by XPS in our experiments is only accurate to $\sim 5 \times 10^{13}$ molecules/cm^2 as there is no independent calibration of coverage, such as LEED. The XPS–IR data agree with the power law correlation of Bradshaw and Hayden's data up to a CO coverage of 8.0×10^{14} molecules/cm^2, which was found to be the saturation coverage of CO on the foil surface at pressures below 10^{-5} mBar and 300 K. Bradshaw and Hayden found on Pt(111) the relationship given above failed for coverages $> 5 \times 10^{14}$ molecules/cm^2. In their experiments at high coverages and low temperatures (<150 K) the CO formed ordered islands where strong dipole coupling resulted in the integrated absorption intensity being almost independent of coverage. Apparently, in our experiments, at higher temperatures and on the less perfect foil substrate, adsorbate ordering was less significant. This resulted in the infrared intensity being more sensitive to surface coverage over a broader range of coverages in the experiments reported here. Surface coverages, θ, reported in this paper are the surface coverage normalized by the saturation coverage at 300 K. Equation (2) was used to determine CO coverages from our infrared data, which assumes the absorption coefficient of CO adsorbed on on-top sites on Pt is not dependent on crystal structure, which has been suggested by Hayden et al. based on studies on stepped Pt surfaces (*14*). We have also assumed the absorption coefficient is not affected by co-adsorbates such as N, NO, and O. Previously it has been observed that co-adsorbates do affect the absorption coefficient of CO (*52*); this is a secondary effect and in the absence of quantitative models it was neglected.

When the surface coverage, θ_{CO}, undergoes a small perturbation, the infrared absorption intensity variation at frequency ν is given by

$$\frac{\partial I(\theta_{CO}, t)}{\partial t} = I \left\{ \frac{\nu - \bar{\nu}}{\sigma^2} \frac{d\bar{\nu}}{d\theta_{CO}} + \frac{d \ln A}{d\theta_{CO}} \right\} \frac{d\theta_{CO}}{dt}. \quad (3)$$

For small modulations in the surface coverage the variation of peak frequency and peak amplitude with coverage are nearly constant. As seen in the data shown in Fig. 2 there is an absorption frequency, ν^*, for which the intensity variation vanishes (referred to as the demodulation frequency).

This occurs when the bracketed term in Eq. (3) equals zero. One can then show that the variation in coverage is given by

$$\frac{d\theta_{CO}}{dt} = \frac{d \ln I}{dt} \Big/ \frac{d \ln A}{d\theta_{CO}} \left\{ 1 - \frac{\nu - \bar{\nu}}{\nu^* - \nu} \right\}, \quad (4)$$

where $d \ln A/d\theta_{CO}$ is evaluated at the static surface coverage $\bar{\theta}_{CO}$ given by Eq. (2) and $d \ln I/dt$ is evaluated at the infrared absorption frequency ν. The intensity and coverage variations may be expanded in Fourier series based on the modulation frequency, ω, of the molecular beam.

At the fundamental frequency the modulated coverage variation is related to the modulated intensity variation by

$$\theta_{CO}(\omega) = \frac{I(\nu, \omega)}{I(\nu)} \Big/ \frac{d \ln A}{d\bar{\theta}_{CO}} \left\{ 1 - \frac{\nu - \bar{\nu}}{\nu^* - \bar{\nu}} \right\}, \quad (5)$$

where $\bar{I}$ and $\bar{\theta}$ are the steady state values of the absorption intensity at frequency ν and coverage. The modulated coverage variation at a given temperature and pressure was determined from each of the dynamic spectra in a set (as illustrated in Fig. 2) and averaged. The quality of the fit of the data by the shifting gaussian peak model may be assessed by looking at the change in ir absorption intensity as a function of infrared frequency and time during the desorption half cycle, such a comparison is shown in Fig. 4.

During CO adsorption/desorption, when the variation in coverage is small, the kinetics may be linearized around the steady state value. Adsorption/desorption may be described by mass action kinetics for adsorption onto a lattice (Langmuir model),

$$\frac{d\theta_{CO}}{dt} = k_a(1 - \theta_{CO})p_{CO} - k_d\theta_{CO}, \quad (6)$$

where k_a and k_d are the adsorption and desorption rate constants respectively. The steady state coverage is given by

$$\bar{\theta}_{CO} = \frac{K\bar{p}_{CO}}{1 + K\bar{p}_{CO}}, \quad (7)$$

where $K = k_a/k_d$ is the equilibrium constant

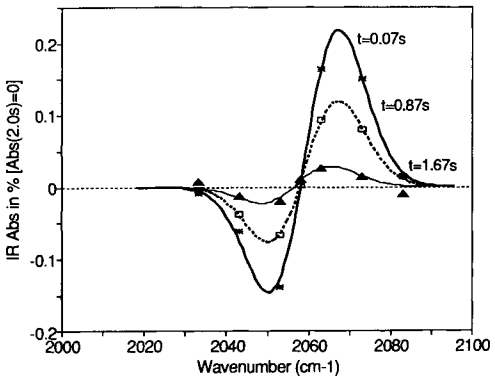

FIG. 4. Variation in infrared absorption as given by the shifting Gaussian Model (Eq. (1)). Modulation frequency 0.25 Hz, T = 450 K, $\bar{p}_{CO} = 9.3 \times 10^{-7}$ mBar, $p_{CO}(\omega) = 7.2 \times 10^{-7}$ mBar, $\bar{\nu}$ = 2059.5 cm^{-1}, ν^* = 2058 cm^{-1}.

for adsorption and $\bar{p}_{CO}$ is the average pressure. The rate constant for desorption, k_d, may be expressed in terms of the average coverage and pressure $\bar{\theta}_{CO}$ and $\bar{p}_{CO}$ the modulation frequency ω, and the modulated coverage and pressure variations, $\theta_{CO}(\omega)$ and $p(\omega)$. Equation (5) can be rearranged to give the rate constant for desorption:

$$k_d = \omega \Big/ \left[\left(\frac{\bar{\theta}_{CO} p(\omega)}{\theta(\omega)\bar{p}_{CO}} \right)^2 - \left(\frac{1}{1 - \bar{\theta}_{CO}} \right)^2 \right]^{1/2}. \quad (8)$$

The rate constant for CO desorption was found at different temperatures and pressures by the following procedure:

(1) The average coverage of CO, $\bar{\theta}_{CO}$, was determined by co-adding two spectra taken while modulating the CO pressure. The two spectra were gated 180° out-of-phase with each other relative to modulated beam.

(2) A series of dynamic spectra were taken at eight IR absorption frequencies. The demodulation frequency, ν^*, was determined. The modulated coverage variation was determined from Eq. (5).

(3) The rate constant for desorption was found from Eq. (8).

Two recent papers have shown the ob-

TABLE 1

CO Adsorption/Desorption Kinetics

Temperature (K)	$\bar{p}_{CO}$ (mBar × 10^7)	$\frac{p_{CO}(\omega)}{\bar{p}_{CO}}$	$\frac{\bar{\theta}_{CO}(T)}{\theta_{CO}(300)}$ (Eq. (2))	$\frac{\theta_{CO}(\omega)}{\bar{\theta}_{CO}}$ (Eq. (6))	k_d (sec^{-1}) (Eq. (10))
326	2.2	0.60	0.98	0.001	4.3×10^{-4}
382	2.2	0.60	0.94	0.028	7.3×10^{-3}
399	2.2	0.60	0.93	0.048	1.5×10^{-2}
426	2.2	0.60	0.87	0.093	4.3×10^{-2}
428	2.2	0.60	0.83	0.117	4.1×10^{-2}
450	2.2	0.60	0.70	0.206	7.7×10^{-2}
453	2.2	0.60	0.48	0.216	9.1×10^{-2}
458	2.2	0.60	0.30	0.240	1.1×10^{-1}
466	2.2	0.60	0.15	0.341	1.8×10^{-1}
488	2.2	0.60	0.02	1.914	5.7×10^{-1}
428	9.3	0.88	0.88	0.152	3.3×10^{-2}
450	9.3	0.88	0.76	0.129	4.3×10^{-2}
458	9.3	0.88	0.70	0.473	1.0×10^{-1}

served rate constant for desorption is slightly different from the true rate constant due to variations of the adsorption and desorption rate constants with coverage (*53, 54*). We have not attempted to correct the data for this effect because the corrections require detailed information about the rate constants as functions of coverage. One must have either a quantitative model to obtain this information or else extensive data as a function of coverage is required. Surface coverage is not an independent parameter and such data requires data at many pressures and temperatures, which are not presently available.

The experimental results for CO adsorption/desorption with the CO beam modulated at 0.25 Hz are summarized in Table 1. At each experimental condition of temperature and average CO pressure, $\bar{p}_{CO}$, we report the modulated pressure variation, the average CO surface coverage normalized to saturation, the normalized CO coverage variation and the apparent first order rate constant for desorption. An Arrhenius plot of the rate constant for desorption, shown in Fig. 5, revealed that the activation energy for desorption and the pre-exponential factor changed dramatically from 488 to 325 K. At the higher sample temperatures the data was fit by an activation energy was 36 kcal/mole with a pre-exponential factor of 10^{15} sec^{-1}, which agree well with the results of previous investigators (*6–9*). At the low surface temperatures the apparent activation energy was 14 kcal/mol, and the pre-exponential factor 10^5 sec^{-1}. We believe this change in kinetic parameters for desorption results from repulsive interactions between adsorbed CO molecules, which reduces the

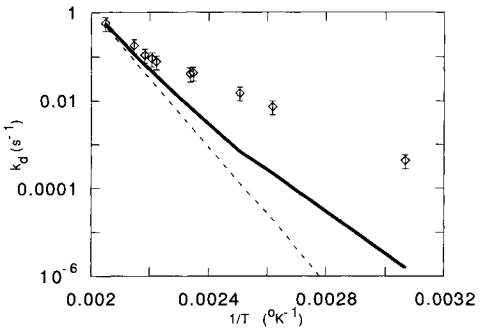

FIG. 5. Isobaric Arrhenius plot of k_d for CO desorption. $\bar{p}_{CO} = 2.2 \times 10^{-7}$ mBar. Dashed line is for noninteracting adsorbates, $k_d = 10^{15}\, e^{-18{,}000/T}$ sec^{-1}. Solid line is for quasi-chemical approximation with 6 nearest neighbors and repulsive interaction energy of 1.5 kcal/mol and $k_d = 10^{15}\, e^{-18{,}000/T}$ sec^{-1}.

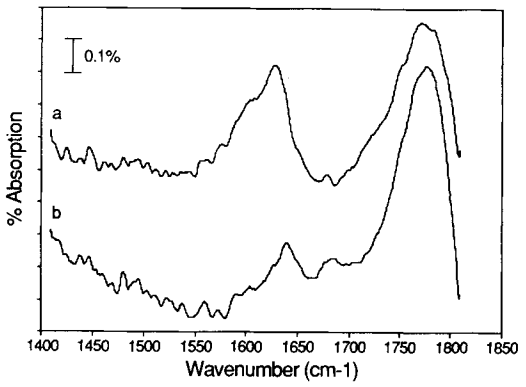

FIG. 6. Static ir spectra of NO adsorbed on Pt foil at 330 K. (a) $\bar{p}_{NO} = 1.3 \times 10^{-6}$ mBar; (b) $\bar{p}_{NO} = 1.3 \times 10^{-2}$ mBar.

adsorption energy with increasing CO coverage.

(ii) NO Adsorption/Desorption

The adsorption/desorption of NO could not be studied quantitatively by following the dynamic behavior of the NO IR absorption bands. NO decomposed above 400 K to adsorbed oxygen and nitrogen. X-ray photoelectron spectra of the surface after exposure to NO between 400 and 500 K showed the buildup of surface oxygen, and in the absence of hydrogen or CO to react with surface oxygen, the oxygen remained adsorbed to above 700 K. The slow buildup of adsorbed atomic species caused the surface to change; we were unable to reproduce surface conditions at different temperatures and beam pressures. Previous IR studies of NO adsorbed on Pt also showed the peaks changed nonreversibly when the temperature was cycled between 400–500 K, presumably due to surface reconstruction and NO decomposition (*26–28*).

Static IR spectra of NO adsorbed on the Pt foil were obtained at 330 K, below the temperature for NO dissociation. Figure 6 show the spectra taken at NO pressures of 1.3×10^{-6} mBar and 1.3×10^{-2} mBar. These spectra are noisier than the CO spectra. They were taken with the HgCdTe detector, which has a poorer response than the InSb detector used above 1850 cm^{-1}; the absorption coefficient of NO adsorbed is also weaker than that of CO. At the lower NO pressure two IR absorption bands were observed of nearly equal intensity at 1630 and 1770 cm^{-1}. Increasing the NO pressure reduced the intensity of the IR band at 1630 cm^{-1} and increased the intensity of the IR band at 1770 cm^{-1}. The total integrated infrared intensity in the two bands remained nearly constant with the increased pressure.

NO absorption bands at similar frequencies to those reported here have been observed on Pt foils, Pt(100) and Pt(110). Both bands are attributed to on-top adsorption with the NO axis tilted relative to the surface (*29, 34*). The band 1630 cm^{-1} was observed for low temperature adsorption and was attributed to adsorption on restructured Pt surfaces (*34*). As the temperature was raised the surface structure was assumed to relax and the NO band is observed at 1770 cm^{-1}. The data reported here suggest that increased NO pressures can also induce the relaxation of the surface reconstruction.

The surface coverage of NO was estimated from the integrated IR intensities. It was assumed that the absorption coefficients of NO for the both bands were the same and equal to the value obtained by Hayden on Pt(111) (*30*). Hayden's data for the concentration of adsorbed NO, n_{NO}, can be fit by a power law correlation,

$$n_{NO} = 1.5 \times 10^{13}\{\int I(\nu)\, d\nu\}^{0.94} \text{ molecules/cm}^2, \quad (9)$$

where $I(\nu)\, d\nu$ has units %-cm^{-1}. Equation (9) assumes that the NO absorption coefficients are independent of adsorption site and surface coverage. This assumption implies that the NO surface coverage at 300 K did not change between 10^{-6} and 10^{-2} mBar, suggesting the surface was saturated, and the changes in the IR spectra were due to reconstruction of the surface. The NO surface coverage at 300 K and 10^{-6} mBar was assumed to be saturation coverage and NO surface coverages were normalized to that

coverage. XPS was also used as an independent calibration of the NO surface coverage. The IR and XPS results agreed to 1×10^{14} molecules/cm^2, which is an error of 0.05 monolayer in the coverage determination of NO.

The complexities of NO decomposition and adsorbate induced reconstruction resulted in very complex dynamic IR spectra. The IR band at 1770 cm^{-1} showed simple behavior, the absorption intensity increased at all frequencies with increased NO coverage. In-phase and out-of-phase responses were observed for the infrared band circa 1630 cm^{-1} and may indicate dipole coupling or could result from more complex surface processes. At this time we are unable to provide a reasonable model to account for the dynamic NO spectra. Our primary interest in the NO spectra was to estimate the NO surface coverage during the CO/NO reaction.

(iii) The CO/NO Reaction

The reaction of CO and NO on Pt was examined by maintaining a constant background pressure of 10^{-7}–10^{-6} mBar of one gas while the pressure of the other gas was modulated. Within the experimental constraints of keeping the total pressure less than 1×10^{-5} mBar (to avoid overloading the pumping system), and having a minimum beam flux of $\sim 1 \times 10^{-7}$ mBar (to be substantially above the background pressure), our studies were restricted to temperatures $430 < T < 470$ K. Under these conditions both CO and NO were adsorbed at measurable surface concentrations to permit the dynamics of their surface coverages to be followed with RIRS. At temperatures below 430 K the surface coverages diminished with time due to adsorbed oxygen and nitrogen from NO decomposition. Surface contamination due to NO decomposition was less severe when CO was coadsorbed with NO. Adsorbed CO apparently facilitated nitrogen atom recombination on the surface and reacted with adsorbed oxygen to help keep the surface clean.

The experiments for the CO/NO reaction were identical to those for CO and NO adsorption/desorption. Averaged CO and NO spectra were taken by co-adding two spectra phase shifted by 180° relative to the modulated beam. Dynamic spectra were taken at a series of frequencies for both CO and NO. The average CO and NO surface concentrations were determined from the integrated intensity of the averaged spectra through the use of Eqs. (2) and (9). The modulated CO coverage variation was determined through the application of Eq. (5) to the modulated IR absorption intensity. The application of Eqs. (2) and (9) to determine the coverages of CO and NO assumes that the presence of NO did not affect the absorption coefficient of adsorbed CO and vice versa. Vibrational coupling between NO and CO is negligible so the primary effect of the coadsorbates is disruption of islanding. As was pointed out above, the higher temperatures used in these experiments on a foil surface minimized the effect of islanding so the infrared absorption intensity was able to give a reasonable measure of adsorbate coverages over the entire range of surface coverages.

For a steady NO pressure and a modulated CO pressure an effective first order rate constant for the removal of CO from the surface was obtained through the application of Eq. (10) to the CO coverage modulation:

$$k_d = \omega \Big/ \left[\left(\frac{\bar{\theta}_{CO} p(\omega)}{\theta(\omega) \bar{p}_{CO}} \right)^2 - \left(\frac{1}{1 - \bar{\theta}_{NO} - \bar{\theta}_{CO}} \right)^2 \right]^{1/2}. \quad (10)$$

We were unable to obtain quantitative results for the NO dynamic spectra because the complexity of the NO absorption peaks inhibited the correlation of intensity modulation to coverage modulation.

NO adsorbed on the surface enhanced the rate of CO removal from the surface. Figure 7 shows the static IR spectra of adsorbed CO with and without a background flux of NO. Superimposed on the static spectra are

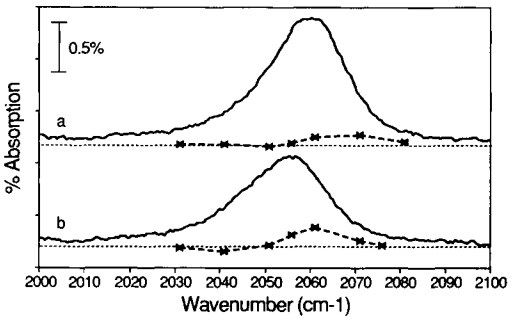

FIG. 7. Static spectra of CO at 428 K (solid lines), CO pressure modulated at 0.25 Hz, with the IR absorption intensity modulations superimposed (dashed lines). $\bar{p}_{CO} = 9.3 \times 10^{-7}$ mBar; $p_{CO}(\omega) = 7.2 \times 10^{-7}$ mBar. (a) $\bar{p}_{NO} = 0$ mBar; (b) $\bar{p}_{NO} = 2.7 \times 10^{-6}$ mBar.

the modulated intensity variations when the CO pressure was modulated. The increased coverage modulation when NO was present is apparent in the larger IR intensity modulations. As the modulation amplitude is proportional to the reaction rate the rate of CO removal is increased by more than a factor of 4 when NO was present.

Modulation of the CO pressure resulted in the modulation of the NO surface coverage as well. With a constant NO pressure and a modulated CO beam, the NO infrared absorption at 1631 and 1794 cm^{-1} decreased when the CO pressure increased due to the CO/NO reaction. Table 2 summarizes and compares the effective rate constant for CO removal from the surface for the conditions of (i) modulated CO pressure and (ii) modulated CO pressure with an NO background. In all cases the rate of CO removal from the surface increased due to coadsorbed NO. Under the conditions studied the effective first order rate constant for CO removal increased by a factor of 3 to 7. The normalized CO and NO surface coverages at the reaction conditions are also summarized in Table 2.

When the roles of NO and CO were reversed, providing a constant CO pressure and a modulated NO pressure the CO coverages variations increased as indicated by the dynamic spectra shown in Fig. 8. When the NO pressure is modulated and the CO pressure is held constant, there is no simple expression for the effective rate constant of CO removal from the surface. We discuss below the use of this data to extract rate constants for the CO/NO reaction based on different reaction mechanisms.

DISCUSSION

Molecular beam techniques permit one to measure steady state reaction kinetics without complications of transport limitations in the gas phase. Modulated beams give improved signal discrimination permitting reactive scattering to be distinguished from elastic scattering. The reaction product response can provide information about the reaction mechanism and reaction kinetics. The reader is referred to reviews by Olander and co-workers (*55*), D'Evelyn and Madix (*56*), and Chang and Weinberg (*57*) for experimental details and methods of analysis. Until recently, these modulated beam studies have been limited to low surface coverages (see, for example, Refs. (*6–9, 58*)). At these conditions the reaction product response frequently results from reactions at defects rather than an average for the surface (*58*). Furthermore, the effects of adsorbate–adsorbate interactions cannot be addressed.

The unique aspect of the experiments described here is the direct observation of surface coverages and reaction kinetics over a broad range of surface coverages using modulated molecular beams. Recently, Sibener and co-workers introduced a three-beam technique to study kinetics of surface reactions at moderate surface coverages (*54, 59, 60*). In their work, He scattering was used to characterize the coverage of adsorbed CO during CO adsorption/desorption (*54*). This is a promising development but is difficult to implement with co-adsorbed reactants. We have chosen to follow surface coverages directly with infrared spectroscopy. This has the advantage of being able to follow the surface coverage of different species in a reaction system unam-

TABLE 2

CO Removal Kinetics with CO/NO Coadsorption

Temperature (K)	$\bar{p}_{CO}$ (mBar × 10^7)	$\frac{p_{CO}(\omega)}{\bar{p}_{CO}}$	$\bar{p}_{NO}$ (mBar × 10^7)	$\frac{\bar{\theta}_{CO}(T)}{\theta_{CO}(300)}$ (Eq. (2))	$\frac{\bar{\theta}_{NO}(T)}{\theta_{CO}(300)}$ (Eq. (11))	$\frac{\theta_{CO}(\omega)}{\bar{\theta}_{CO}}$ (Eq. (6))	k_d (sec^{-1}) (Eq. (10))
428	2.2	0.60	0.0	0.83	0.0	0.117	4.1×10^{-2}
428	2.2	0.60	27.0	0.20	0.40	0.353	1.7×10^{-1}
428	9.3	0.88	0.0	0.88	0.0	0.152	3.3×10^{-2}
428	9.3	0.88	27.0	0.24	0.24	0.378	1.8×10^{-1}
450	2.2	0.60	0.0	0.70	0.0	0.206	7.7×10^{-2}
450	2.2	0.60	27.0	0.078	0.45	0.512	2.3×10^{-1}
450	9.3	0.88	0.0	0.76	0.0	0.129	4.3×10^{-2}
450	9.3	0.88	27.0	0.18	0.29	0.702	2.4×10^{-1}
458	2.2	0.60	0.0	0.30	0.0	0.240	1.1×10^{-1}
458	2.2	0.60	27.0	0.014	0.31	0.753	3.0×10^{-1}
458	9.3	0.88	0.0	0.70	0.0	0.473	1.0×10^{-1}
458	9.3	0.88	27.0	0.071	0.25	1.958	4.1×10^{-1}

biguously. The major limitation with our present experimental configuration is that we are unable to monitor the gas phase reaction product, so the rates of reaction are based on the rates of removal of species from the surface. Other difficulties with the infrared technique are the nonlinear absorption coefficient and peak shifts with coverage and the effect of co-adsorbates on the absorption coefficient. However, vibrational spectroscopies are far superior to any other technique for identifying different surface species unambiguously. Furthermore, infrared spectroscopy does not require UHV to operate, which makes it potentially more robust than electron spectroscopies. The studies reported here are at pressures several orders of magnitude greater than typical UHV conditions ($P < 10^{-9}$ mBar), and the pressure limitations in these studies resulted from vacuum pumping and not the spectroscopy. Discussed below are the new findings from this study concerning the kinetics of CO desorption as a function of surface coverage and the kinetics of the CO/NO reaction.

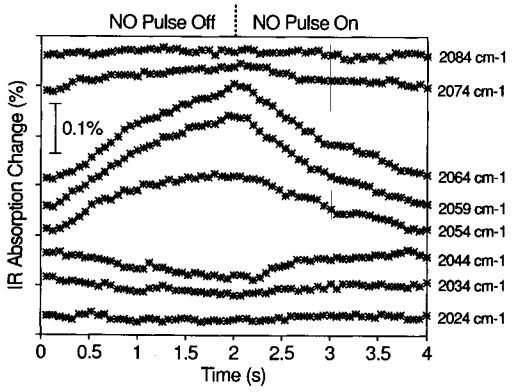

FIG. 8. Dynamic infrared spectra of CO at 465 K due to CO/NO reaction with steady CO pressure, $\bar{p}_{CO} = 1.3 \times 10^{-6}$ mBar, and NO pressure modulated at 0.25 Hz, $\bar{p}_{NO} = 1.2 \times 10^{-6}$ mBar, $p_{NO}(\omega) = 0.9 \times 10^{-6}$ mBar.

(i) *CO Adsorption/Desorption*

The kinetics of CO adsorption and desorption on Pt has been extensively studied (*6–12*). At low coverages the desorption of CO is characterized by a simple first-order process with a pre-exponential factor of $\sim 10^{15}$ sec^{-1} and an activation energy of 36 kcal/mol from surfaces with defects such as steps (*6–10, 12*). The kinetic parameters obtained here at temperatures >460 K, where the surface coverages are $<\frac{1}{2}$ saturation, agree well with those findings. How-

ever, at lower temperatures, where the surface coverage is high, the Arrhenius plot (Fig. 5) shows that the rate constant does not drop off as expected. Instead, the activation energy and pre-exponential factor for CO desorption both decreased. The apparent change in the kinetic parameters could be explained in terms of parallel desorption paths characterized by two different rate constants.

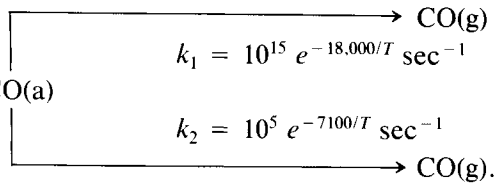

This explanation does not seem reasonable as the infrared spectra show only a single infrared absorption band suggesting that only a single type of adsorbed CO exists.

A more reasonable alternative for the change in rate is that repulsive adsorbate–adsorbate interactions cause the rate of desorption to increase with increasing coverage. Repulsive interactions have been shown to account for decreases in the heat of adsorption with increasing adsorbate coverage (*61–63*) and for increased rates of desorption in thermal desorption (*64–66*). Infrared studies and thermal desorption results both indicate that CO molecules adsorbed in nearest neighbor sites on Pt are repulsive (*10–13*).

The effect of repulsive nearest neighbor interactions on the desorption rate can be estimated with the quasi-chemical approximation (*65–67*).

We have calculated the isobaric desorption rate of CO as a function of temperature corresponding to our experimental parameters using the quasi-chemical approximation. Figure 5 shows the experimental data plotted with two lines, the dashed line corresponds to no interaction between adsorbed species, and the solid line corresponds to an interaction energy of 1.5 kcal/mol (4% of the adsorption energy). The model shows that repulsive interactions increase the desorption rate relative to the desorption rate with no interactions. As temperature decreases at constant pressure the desorption rate increase was enhanced due to increasing coverage.

The quasi-chemical model predicts qualitatively the proper trends in the data, indicating a decrease in the apparent activation energy and pre-exponential factor at as temperature decreased at constant pressure. We were unable to get quantitative agreement without treating pressure as an independent parameter. One might suspect that increasing the interaction energy, ω, would improve the fit to the data. This is not so. Increasing the interaction energy above 1.5 kcal/mol causes the apparent rate constant to approach the rate constant with no interactions. As the repulsive interactions increase they preclude adsorption in nearest neighbor sites at a fixed pressure, so the coverage saturates with no nearest neighbor sites occupied. With no nearest neighbor sites occupied the repulsive interactions do not affect the rate of desorption. The experimental data may be better fit by models that account for interactions beyond the nearest neighbor. IR data shows that CO dipoles interact resulting in a frequency shift of the absorption peak. Dipole interactions are long range and a model that only considers nearest neighbor interactions is not expected to be quantitative. Recently, Peterson and Kevan have expanded a virial approximation for a lattice gas that can account for longer range adsorbate–adsorbate interactions (*70*). This is a simpler alternative to the renormalization group approximations of which the quasi-chemical approximation is a simple case. The virial expansions do not converge rapidly (*68*) so this approach works best at low surface coverages, where Peterson and Kevan applied this approach (*70*).

It is also possible to extract adsorption rate constants for the CO adsorption/desorption data. Most frequently, adsorption studies report a sticking probability, which is the fraction of incident molecules that ad-

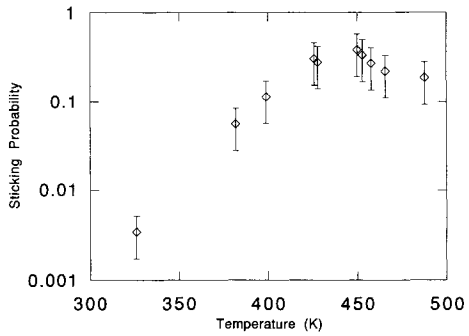

FIG. 9. Isobaric sticking coefficient of CO as a function of temperature. $\bar{p}_{CO} = 2.2 \times 10^{-7}$ mBar; $p_{CO}(\omega) = 1.3 \times 10^{-7}$ mBar.

sorb on a surface. The sticking probability, $S(\theta)$, is given by,

$$S_{CO}(\theta) = \frac{k_d \bar{\theta}_{CO}}{\bar{p}_{CO}}. \quad (11)$$

The isobaric sticking probability determined from the data summarized in Table 1 are plotted as a function of temperature in Fig. 9. The sticking probability is nearly constant for $488 > T > 430$ K, where the surface concentration is less than 70% saturation. This is consistent with a mobile precursor for CO adsorption, which has been suggested by a number of previous studies (*5–11*). The data also suggest the low coverage sticking probability is not very temperature sensitive. At temperatures $T < 400$ K, where the surface coverages approach saturation the sticking probability drop off. The limited data indicate the sticking probability decreases more rapidly than $(1 - \theta)$ at low temperatures/high coverages, suggesting the repulsive interactions affect the sticking probability.

(ii) CO/NO Surface Reaction

A number of investigations of the CO/NO reaction have been carried out. Most of these studies have found the reaction to be first order in NO pressure and negative order in CO (*42–51*). Based on these findings most investigators concluded that NO dissociation (step 3 below) was the rate limiting step in the CO/NO reaction to CO_2 and N_2.

$$CO(g) + * \xrightarrow{1} CO*$$

$$NO(g) + * \xrightarrow{2} NO*$$

$$NO* + * \xrightarrow{3} N* + O*$$

$$CO* + NO* \xrightarrow{4} CO_2(g) + N* + *$$

$$2N* \xrightarrow{5} N_2(g) + 2*$$

$$CO* + O* \xrightarrow{6} CO_2(g) + 2*.$$

However, Klein *et al.* (*50*) carried out extensive studies varying pressure over eight orders of magnitude, temperature variations over 800 K and CO/NO ratios from 0.0005 to 100 and suggested that the rate was always consistent with a bimolecular surface reaction (step 4 above) being rate limiting. Our experimental results for the coverage variations during the CO/NO reaction further support the idea of the bimolecular reaction being rate limiting.

The data given in Table 2 show that the rate of CO removal from the surface is 3–7 times greater due to the CO/NO reaction than due to CO desorption. If CO and NO removal from the surface is assumed to only result from the CO/NO reaction, r, one can write expressions for the coverage changes of CO and NO:

$$\frac{d\theta_{CO}}{dt} = k_a p_{CO}(1 - \theta_{CO} - \theta_{NO}) - r \quad (12a)$$

$$\frac{d\theta_{NO}}{dt} = k_a p_{NO}(1 - \theta_{CO} - \theta_{NO}) - r. \quad (12b)$$

In Eqs. (12) the desorption of CO and NO have been neglected relative to the reaction of CO and NO. It is possible that the enhanced rate of CO removal from the surface was due to repulsive interactions between CO and NO, causing the CO desorption rate to increase. The kinetics of CO removal in this instance would be similar to the bimolecular reaction case (reaction step 4 above).

TABLE 3

CO/NO Reaction Kinetics for Modulated Molecular Beam Experiments

Rate-limiting step	NO Dissociation	Bimolecular reaction
Rate of surface reaction CO coverage modulation	$r = k_r\theta_{NO}(1 - \theta_{CO} - \theta_{NO})$	$r = k_r\theta_{CO}\theta_{NO}$
p_{NO} constant p_{CO} modulated	$\theta_{CO}(\omega) = \dfrac{k_r\bar{\theta}_{NO}p_{CO}(\omega)(1 - \bar{\theta}_{CO} - \bar{\theta}_{NO})}{\omega\bar{p}_{CO}}$	$\theta_{CO}(\omega) = \dfrac{k_r\bar{\theta}_{NO}\bar{\theta}_{CO}p_{CO}(\omega)}{\omega\bar{p}_{CO}}\sqrt{1 + \left[\dfrac{k_r\bar{\theta}_{CO}(1 - \bar{\theta}_{CO})}{\omega(1 - \bar{\theta}_{CO} - \bar{\theta}_{NO})}\right]^2} \Big/ \sqrt{1 + \left[\dfrac{k_r\{\bar{\theta}_{CO}(1 - \bar{\theta}_{CO}) + \bar{\theta}_{NO}(1 - \bar{\theta}_{NO})\}}{\omega(1 - \bar{\theta}_{CO} - \bar{\theta}_{NO})}\right]^2}$
p_{NO} modulated p_{CO} constant	$\theta_{CO}(\omega) = \dfrac{(K_r/\omega)^2(1 - \bar{\theta}_{CO} - \bar{\theta}_{NO})^2\bar{\theta}_{NO}p_{NO}(\omega)}{\sqrt{1 - (k_r/\omega)^2(1 - \bar{\theta}_{CO} - \bar{\theta}_{NO})^2\bar{p}_{NO}}}$	$\theta_{CO}(\omega) = \dfrac{(k_r/\omega)^2\bar{\theta}_{CO}(1 - \bar{\theta}_{CO}(1 - \bar{\theta}_{CO})\bar{\theta}_{NO}\bar{\theta}_{CO}p_{NO}(\omega)}{(1 - \bar{\theta}_{CO} - \bar{\theta}_{NO})\bar{p}_{NO}} \Big/ \sqrt{1 + \left[\dfrac{k_r\{\bar{\theta}_{CO}(1 - \bar{\theta}_{CO}) + \bar{\theta}_{NO}(1 - \bar{\theta}_{NO})\}}{\omega(1 - \bar{\theta}_{CO} - \bar{\theta}_{NO})}\right]^2}$

The background gas composition during the experiments was checked by mass spectroscopy and the CO_2 pressure increased during the CO/NO reaction experiments, indicating that at least a portion of the CO removal was due to the CO/NO reaction; however, we cannot quantify the fraction of CO oxidized to CO_2 with our current experimental configuration.

Table 3 summarizes the rate of reaction and the functional form for the amplitude of the modulated CO coverage for the two possibilities of NO dissociation or a bimolecular reaction between NO and CO being rate limiting. In the expressions for CO coverage modulation, $\theta_{CO}(\omega)$, everything is known except the rate constant for the surface reaction. The rate constants for the two different mechanisms and all the different data sets were evaluated and are presented in Tables 4 and 5.

In the experiments where the CO pressure is modulated and the NO pressure is constant (Table 4), the experimental data for the rate constants are only consistent with the bimolecular reaction mechanism. The rate constants k_{bimol} are mutually consistent at different levels of CO modulation and they also increase with increasing temperature as expected. The rate constants based on NO dissociation being rate-limiting are not constant for different levels of CO modulation and they do not vary with temperature. These consistency checks on the rate constant suggest that the rate-limiting step during the CO modulation experiments is the bimolecular surface reaction between NO and CO. It should be reiterated here that CO displacement by NO will give qualitatively the same response as a bimolecular CO/NO reaction. The data cannot rule out the possibility of NO dissociation being rate-limiting for CO oxidation, but the oxidation reaction occurs at a lesser rate than CO displacement.

The NO modulation experiments are very revealing concerning the reaction mechanism. When NO dissociation is rate-limiting, the CO coverage modulation amplitude, given by the expression in Table 3, always decreases with increasing CO coverage, $\bar{\theta}_{CO}$, and hence with increasing CO pressure. This is contrary to the data at 465 K, where the rate increased with increasing

TABLE 4

CO/NO Reaction Kinetics with CO Pressure Modulation[a]

Temperature (K)	$\bar{p}_{CO}$ (mBar × 10^7)	$\frac{p_{CO}(\omega)}{\bar{p}_{CO}}$	$\frac{\bar{\theta}_{CO}(T)}{\theta_{CO}(300)}$	$\frac{\bar{\theta}_{NO}(T)}{\theta_{CO}(300)}$	$\frac{\theta_{CO}(\omega)}{\bar{\theta}_{CO}}$	k_{dis}[b]	k_{bimol}[c]
428	2.2	0.60	0.20	0.40	0.353	0.18	0.68
428	9.3	0.88	0.24	0.24	0.378	0.21	0.69
450	2.2	0.60	0.078	0.45	0.512	0.08	1.29
450	9.3	0.88	0.18	0.29	0.702	0.23	1.26
458	2.2	0.60	0.014	0.31	0.753	0.03	6.70
458	9.3	0.88	0.071	0.25	1.958	0.23	6.25

[a] Constant NO pressure of 2.7×10^{-6} mBar.
[b] Rate constant for NO dissociation being rate-limiting.
[c] Rate constant for bimolecular reaction between CO and NO being rate-limiting.

CO pressure (see Table 5), indicating NO dissociation cannot be rate-limiting under those reaction conditions. In contrast, if the bimolecular reaction is rate-limiting, the CO coverage modulation will decrease with increasing CO pressure when the total coverage, $\bar{\theta}_{CO} + \bar{\theta}_{NO}$, is high (corresponding to lower temperatures), and will increasing with increasing CO pressure when the total coverage is low (corresponding to higher temperatures). These trends in the CO coverage modulations are consistent with the experimental results.

The rate constants for the bimolecular reactions are also mutually consistent for the NO modulation experiments at different CO pressures, whereas the rate constants for NO dissociation being rate-limiting are inconsistent. Lastly, the rate constants for the bimolecular rate constants are self consistent as a function of temperature for the combined experimental data sets of either NO modulation or CO modulation. Under all conditions studied here, the data are consistent with the bimolecular reaction between adsorbed CO and adsorbed NO being the rate-limiting step in the CO/NO reaction, consistent with the previous work or

TABLE 5

CO/NO Reaction Kinetics with NO Pressure Modulation

Temperature (K)	$\bar{p}_{CO}$ (mBar × 10^7)	$\frac{p_{NO}(\omega)}{\bar{p}_{NO}}$[a]	$\frac{\bar{\theta}_{CO}(T)}{\theta_{CO}(300)}$	$\frac{\bar{\theta}_{NO}(T)}{\theta_{CO}(300)}$	$\frac{\theta_{CO}(\omega)}{\bar{\theta}_{CO}}$	k_{dis}[b]	k_{bimol}[c]
435	1.3	0.78	0.25	0.47	0.242	0.14	0.35
435	6.6	0.78	0.40	0.24	0.151	0.21	0.42
435	13.0	0.78	0.51	0.10	0.057	0.22	0.36
450	1.3	0.78	0.15	0.37	0.255	0.07	1.40
450	6.6	0.78	0.37	0.18	0.225	0.30	1.33
450	13.0	0.78	0.43	0.08	0.103	0.32	1.32
465	1.3	0.78	0.053	0.36	0.257	0.02	7.45
465	6.6	0.78	0.23	0.10	0.285	0.27	8.03
465	13.0	0.78	0.40	0.09	0.417	0.90	9.07

[a] $\bar{p}_{NO} = 1.2 \times 10^{-6}$ mBar.
[b] Rate constant for NO dissociation being rate-limiting.
[c] Rate constant for bimolecular reaction between CO and NO being rate-limiting.

Klein *et al.* (*50*). Of course one cannot prove a reaction mechanism from the reaction kinetics. It is only possible to say that the data are consistent with the bimolecular reaction mechanism and are not consistent with the NO dissociation mechanism.

There are many possible reaction mechanisms which we have not fully explored for consistency with the data. N_2O has been suggested as an intermediate in the reaction (*71, 72*); the kinetic response for this mechanism would be similar to the bimolecular CO + NO reaction presented above. Another alternative is that step 6 in the mechanism given above could be rate-limiting. This would result in a low NO steady state coverage and no coupling of the modulated CO coverage with NO modulation, which is inconsistent with the experimental results. All these analyses assume a uniform surface reaction, all these conclusions would be invalid if the reactions occur at defects and different defect sites catalyze different reactions. It is the nature of nature of kinetics experiments that one can identify mechanisms consistent with the data, but the data cannot prove a reaction mechanism.

We have not tried to extract activation energies and pre-exponential factors for the CO/NO reaction from our data. The data are over a limited temperature range and the surface coverages of NO are not very accurate so the errors would be too great to make them meaningful. Furthermore, we suspect adsorbate–adsorbate interactions, as observed with CO adsorption/desorption, to be important below 450 K. The adsorbate–adsorbate interactions would generally cause the reaction rate to be greater than expected at high surface coverages due to weaker adsorption bonds for the adsorbates, a hypothesis that is consistent with the data.

Finally, it should be noted that our data showed no evidence for rate oscillations in the CO/NO reaction as have been observed in other studies (*46–49*). The parameter space explored here did not encompass conditions where oscillations have been observed in other studies so we did not expect to see any oscillations.

CONCLUSIONS

This work has demonstrated the utility of dynamic reflection infrared spectroscopy to elucidate the mechanism and kinetics of surface reactions. The isobaric kinetics of CO adsorption/desorption changed as a function of temperature. The desorption rate constant changed from $k_d = 10^{15} e^{-18{,}000/T}$ sec^{-1} at higher temperatures where the surface coverages were less than $\frac{1}{2}$ saturation to $k_d = 10^5 e^{-7000/T}$ sec^{-1} at lower temperatures where the surface coverage approached saturation coverage. Decreases in both the activation energy and preexponential factor for desorption were attributed to repulsive adsorbate–adsorbate interactions.

The dynamic infrared technique indicated that the rate of CO removal during the CO/NO reaction was not consistent with the dissociation of NO being the rate-limiting step but was consistent with a bimolecular reaction between adsorbed CO and adsorbed NO. This was shown under conditions of $428 < T < 465$ K, pressures of 10^{-6} mBar, CO/NO stoichiometries of 0.1 to 2, and was independent of which gas pressure was modulated.

This work demonstrates the utility of infrared spectroscopy to study the kinetics of surface reactions at moderate surface coverages where adsorbate–adsorbate interactions are important. Direct monitoring of the coverages of surface species gives kinetics representative of the average for the surface and not dominated by a small fraction of defect sites on the surface. Ideally one would like to have more extensive data as a function of gas-phase pressure and surface temperature. As more extensive data are obtained the data can be transformed into isosteric (constant coverage) reaction rates that are easier to understand and interpret. Unfortunately surface coverage is not an independent parameter and is determined by the pressure and temperature. In future

work the addition of monitoring the gas phase product species will also help clarify differences in the reaction products from the surface reactions.

ACKNOWLEDGMENTS

The authors thank the Air Force Office of Scientific Research (Grant 86-0217) and the Amoco Foundation for funding the equipment used in these studies. One of us (EWS) thanks the NSF for a fellowship. Lastly, the authors thank the NSF (Grant CTS-8915121) for partial support during the final stages of this work.

REFERENCES

1. Hoffmann, F. M., *Surf. Sci.* **3,** 107 (1983).
2. Benziger, J. B., Preston, R. E., and Schoofs, G. R., *Appl. Opt.* **26,** 343 (1987).
3. Mieher, W. D., Whitman, L. J., and Ho, W., *J. Chem. Phys.* **91,** 3228 (1989).
4. Froitzheim, H., and Schulze, M., *Surf. Sci.* **211/212,** 837 (1989).
5. Reutt-Robey, J. E., Doren, D. J., Chabal, Y. J., and Christman, S. B., *Phys. Rev. Lett.* **61,** 2778 (1988).
6. Fair, J. A., and Madix, R. J., *J. Chem. Phys.* **73,** 3486 (1980).
7. Campbell, C. T., Ertl, G., Kuipers, H., and Segner, J., *Surf. Sci.* **107,** 207 (1981).
8. Lin, T. H., and Somorjai, G. A., *Surf. Sci.* **107,** 573 (1981).
9. Gdowski, G. E., and Madix, R. J., *Surf. Sci.* **115,** 524 (1982).
10. Hopster, H., and Ibach, H., *Surf. Sci.* **77,** 109 (1978).
11. Barth, R., Pitchai, R., Anderson, R. L., and Verykios, X. E., *J. Catal.* **116,** 61 (1989).
12. McClellan, M. R., Gland, J. L., and McFeeley, F. R., *Surf. Sci.* **112,** 63 (1981).
13. Hayden, B. E., and Bradshaw, A. M., *Surf. Sci.* **125,** 787 (1983).
14. Hayden, B. E., Kretzschmar, K., Bradshaw, A. M., and Greenler, R. G., *Surf. Sci.* **149,** 394 (1985).
15. Greenler, R. G., Burch, K. D., Kretzschmar, K., Klauser, R., Bradshaw, A. M., and Hayden, B. E., *Surf. Sci.* **152/153,** 338 (1985).
16. Schweizer, E., Persson, B. N. J., Tushaus, M., Hoge, D., and Bradshaw, A. M., *Surf. Sci.* **213,** 49 (1989).
17. Haaland, D. M., *Surf. Sci.* **185,** 1 (1987).
18. Hammaker, R. M., Francis, S. A., and Eischens, R. P., *Spectrochim. Acta* **21,** 1295 (1965).
19. Shigeishi, R. A., and King, D. A., *Surf. Sci.* **58,** 379 (1976).
20. Crossley, A., and King, D. A., *Surf. Sci.* **95,** 131 (1980).
21. Golden, W. G., Dunn, D. S., Pavlik, C. E., and Overend, J., *J. Chem. Phys.* **70,** 4426 (1979).
22. Gland, J. L., *Surf. Sci.* **71,** 327 (1978).
23. Gorte, R. J., Schmidt, L. E., and Gland, J. L., *Surf. Sci.* **109,** 367 (1981).
24. Gorte, R. J., and Schmidt, L. D., *Surf. Sci.* **111,** 260 (1981).
25. Mantell, D. Z., Cavanagh, R. R., and King, D. S., *J. Chem. Phys.* **84,** 5131 (1986).
26. Dunn, D. S., Severson, M. W., Golden, W. G., and Overend, J., *J. Catal.* **65,** 271 (1980).
27. Dunn, D. S., Severson, M. W., Golden, W. G., and Overend, J., *J. Phys. Chem.* **84,** 336 (1980).
28. Dunn, D. S., Severson, M. W., Hylden, J. L., and Overend, J., *J. Catal.* **78,** 225 (1982).
29. Gorte, R. J., and Gland, J. L., *Surf. Sci.* **102,** 348 (1981).
30. Hayden, B. E., *Surf. Sci.* **131,** 419 (1983).
31. Ibach, H., and Lehwald, S., *Surf. Sci.* **76,** 1 (1978).
32. Gland, J. L., and Sexton, B. A., *Surf. Sci.* **94,** 355 (1980).
33. Bonzel, H. P., and Pirug, G., *Surf. Sci.* **62,** 45 (1977).
34. Pirug, G., Bonzel, H. P., Hopster, H., and Ibach, H., *J. Chem. Phys.* **71,** 593 (1979).
35. Banholzer, W. F., Parise, R. E., and Masel, R. I., *Surf. Sci.* **155,** 653 (1985).
36. Lesley, M. W., and Schmidt, L. D., *Surf. Sci.* **155,** 215 (1985).
37. Banholzer, W. F., and Masel, R. I., *Surf. Sci.* **137,** 339 (1984).
38. Wickham, D. T., Banse, B. A., and Koel, B. E., *Surf. Sci.* **223,** 82 (1989).
39. Brown, M. F., and Gonzalez, R. D., *J. Catal.* **44,** 477 (1976).
40. Morrow, B. A., Chevrier, J. P., and Moran, L. E., *J. Catal.* **91,** 208 (1985).
41. van Slooten, R. F., and Nieuwenhuys, *J. Catal.* **122,** 429 (1990).
42. Lorimer, D., and Bell, A. T., *J. Catal.* **59,** 223 (1979).
43. Lambert, R. M., and Comrie, C. M., *Surf. Sci.* **46,** 61 (1974).
44. Miki, H., Nagase, T., Kioka, T., Sugai, S., and Kawasaki, K., *Surf. Sci.* **225,** 1 (1990).
45. Adlhoch, W., Lintz, H.-G., and Wiesker, T., *Surf. Sci.* **103,** 576 (1981).
46. Schwartz, S. B., and Schmidt, L. D., *Surf. Sci.* **183,** L269 (1987).
47. Bolten, H., Hah, T., LeFoux, J., and Lintz, H. G., *Surf. Sci.* **160,** L529 (1985).
48. Park, Y. O., Banholzer, W. F., and Masel, R. I., *Surf. Sci.* **155,** 341 (1985).
49. Fink, T., Dath, J. P., Basset, M. R., Imbihl, R., and Ertl, G., *Vacuum* **41,** 310 (1990).
50. Klein, R. L., Schwartz, S., and Schmidt, L. D., *J. Phys. Chem.* **89,** 4908 (1985).

51. Banse, B. A., Wickham, D. T., and Koel, B. E., *J. Catal.* **119,** 238 (1989).
52. Benziger, J. B., Myers, A. K., and Schoofs, G. R., *Langmuir* **4,** 268 (1988).
53. Hinch, B. J., and Dubois, L. H., *Chem. Phys. Lett.* **171,** 131 (1990).
54. Perterlinz, K. A., Curtiss, and Sibener, S. J., submitted.
55. Jones, R. H., Olander, D. R., Siekhaus, W. J., and Schwarz, J. A., *J. Vacuum Sci. Technol.* **9,** 1429 (1972).
56. D'Evelyn, M. P., and Madix, R. J., *Surf. Sci. Rep.* **3,** 413 (1984).
57. Chang, H.-C., Weinberg, W. H., *Surf. Sci.* **72,** 617 (1978).
58. Engel, T., *J. Chem. Phys.* **69,** 373 (1978).
59. Padowitz, D. F., and Sibener, S. J., *J. Vacuum Sci. Technol. A*, in press.
60. Padowitz, D. F., Peterlinz, K. A., and Sibener, S. J., submitted.
61. Tracy, J. C., and Palmberg, P. W., *J. Chem. Phys.* **51,** 4852 (1969).
62. Tracy, J. C., *J. Chem. Phys.* **56,** 2736 (1972).
63. Ertl, G., Neumann, M., and Streit, K. M., *Surf. Sci.* **64,** 393 (1977).
64. Goymour, C., and King, D. A., *J. Chem. Soc. Faraday Trans. 1* **69,** 749 (1974).
65. King, D. A., and Wells, M. G., *Proc. R. Soc. London Ser. A* **339,** 245 (1974).
66. Adams, D. L., *Surf. Sci.* **42,** 12 (1974).
67. Guggenheim, E. A., "Mixtures," Oxford Univ. Press, London, 1952.
68. Hill, T. L., "An Introduction to Statistical Thermodynamics," Addison-Wesley, Reading, MA, 1960.
69. Benziger, J. B., and Schoofs, G. R., *J. Phys. Chem.* **88,** 4439 (1984).
70. Peterson, L. D., and Kevan, S. D., *J. Chem. Phys.* **94,** 2281 (1991).
71. Cho, B. K., Shanks, B. H., and Bailey, J. E., *J. Catal.* **115,** 486 (1989).
72. McCabe, R. W., and Wong, C., *J. Catal.* **121,** 422 (1990).